Simulating a Penning trap containing singly-charged calcium ions

Einar Skoglund, Emil J. Kvernevik
(Dated: October 24, 2023)

In this study we investigate the Penning trap - a device to contain and store charged particles. For the purposes and scope of our study, we rely on a simulated model instead of an actual Penning Trap. The trap's working principle is based on the interactions between charged particles and electromagnetic fields, and the play of forces acting on the charges. The motion of the particles is derived numerically, using two numerical methods: the Forward-Euler (FE), and RungeKutta4 (RK4). An analytical solution was also implemented, in order to see how well our numerically derived solutions align with expected values. Methods to enforce additional conditions, such as Coulomb interactions and a time-dependent electric potential were then implemented to improve the realism of the model; the implementation of the Coulomb interaction did not give reasonable results, while the latter revealed resonance frequencies for the Penning trap-particle system. The resonances frequencies being $0.4, 0.7, 1.4, 2.2$ MHz. Having run simulations on one particle using both numerical methods, RK4 was revealed to be the superior method and was used for the rest of the trajectory simulations. Simulations of two or more particles were then ran, the aim being to (i) plot the relative error, and (ii) find the error convergence rates for both methods. We found that for the FE-method, the error convergence rate $r_{err} \approx 1.4$, while for the RK4-method, it was substantially less, at $r_{err} \approx 1.0$.

The GitHub repository for this article can be found at https://github.uio.no/emiljk/FYS3150.git.

I. INTRODUCTION

The study of charged particle motion in electromagnetic fields has played a pivotal role in advancing our understanding of various phenomena in the realm of physics; ranging from particle accelerators, to the behavior of charged particles in space. One of systems that offer us valuable insights into the dynamics of charged particles, is the Penning trap.

The Penning trap is a particle trap, that employs electromagnetic fields to contain and store charged particles - allowing for precise control and study of how they interact with the surrounding fields. Penning traps boast an extensive variety of practical applications, ranging from precision mass spectrometry, to quantum computing, to antimatter research. In fact, this year (2023) Penning traps have been used in the discovery of the effect gravity has on the motion of antimatter [1].

In this study, we seek to simulate the behavior of positively charged particles when confined within a Penning trap, and understand the mechanisms by which the particle trap sustains their confinement. For the scope of this study, we focus on specific case of singly-charged calcium ions Ca^+, and create a simplified model to capture some of the most important attributes of a Penning trap. While it is well established that confining a single charged particle in a Penning trap is a challenging yet achievable endeavor, our study takes a broader approach. We will delve into the intriguing question of how efficient a Penning trap can be at confining larger populations of similar charged particles. In order to address this complex scenario, our model of the particle trap is incumbent on a numerical method that is sturdy enough to simulate the confinement of the particles accurately.

By applying two numerical methods, the Forward-Euler and the 4th order Runge-Kutta, and a variety of computational techniques, we can model the behavior of the charged particles and compare the efficiency of each numerical method. By creating a simplified model of the Penning trap, we aim to gain valuable insights into and a deeper understanding of the complex interactions that occur within a Penning trap. We investigate the effects of Coulomb interactions between the particles, and how a time-dependent electric field can reveal resonance frequencies of the system.

II. METHOD

A. Deriving an analytic solution

To accurately simulate a Penning trap and it's confined particles, we need to know how the particle trap works, and additionally we also need an analytic solution of the particle trajectories - this gives us a baseline to compare our results with, and illustrates how well our model aligns with analytical values.
The penning trap uses electromagnetic fields to store charged particles within itself. The force acting on the particles from these fields, from which we will derive the particles' motion, is incumbent on the Lorentz force:

$$\mathbf{F} = q\mathbf{E} + q\mathbf{v} \times \mathbf{B}, \tag{1}$$

where q is the charge of the particles, $\mathbf{E}$ is the electric field and $\mathbf{B}$ is the magnetic field.
By enforcing that the magnetic field only exerts force on

the particles in the z-direction, we know by default that a particle with a general velocity $\mathbf{v}$ will follow the trajectory of a spiral moving around the z-axis. In the special case when $\mathbf{v}$ is perpendicular to $\mathbf{B}$, the trajectory will be a circle in the xy-plane. By setting the Lorentz force, which will be $\mathbf{F} = q\mathbf{v} \times \mathbf{B}$ when only a magnetic field is present, equal to the centripetal force mv^2/r, where m is the mass of the particle and r is the radius of the circular motion, we can derive [2] the **cyclotron frequency**, $\omega_0 = v/r$, as

$$\omega_0 = \frac{qB_0}{m}, \tag{2}$$

where B_0 is the magnetic field strength. Seeing as it is independent of the particle's velocity, measurements of the cyclotron frequency can be used to determine the particle mass. The way that this is done, is by applying a time dependent electric potential with a given frequency, and then measuring how the particle now changes its orbit. A more extensive description of this phenomena as well as an implementation will be discussed in the simulation part of the methods section.
However, we still need an electric field to trap the particle in the z-direction, this is done by inducing an electric field from electrodes above, under and around the particle. The specific configuration of this Penning trap is shown in FIG 1. Here the electric field is generated by two electrode end caps (a) and an electrode ring (b), while the magnetic field is generated from a cylinder (c) outside the electrodes.

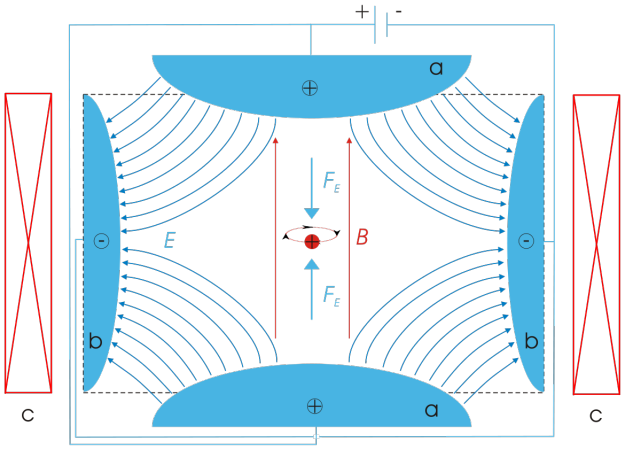

FIG. 1. An illustration of a cross section of a Penning trap, made by Arian Kriesch and taken from Wikimedia Commons. The blue electrodes (a and b) is the source of an electric field that traps the particle (red dot) in the vertical z-direction. The cylinder (c) creates a magnetic field that causes the particle to move in a circular motion in the horisontal xy-plane.

For the purposes of the first part of this study, we will consider an ideal penning trap, where we use the constant electric potential

$$V(x, y, z) = \frac{V_0}{2d^2}\left(2z^2 - x^2 - y^2\right), \tag{3}$$

where V_0 is the applied potential to the electrodes, and d is the characteristic dimension of the penning trap, defined as $d = \sqrt{z_0^2 + r_0^2/2}$, where z_0 is the distance from the center to the end caps and r_0 is the distance to the ring. From the electric potential we then calculate the electric field as

$$E(x, y, z) = -\nabla V = \frac{V_0}{d^2}(x + y - 2z). \tag{4}$$

As the force generated from the electric field is proportional to the displacement in the z-direction, the trajectory of the particles will, in addition to the circular motion in the xy-direction, have a spring-like motion in the z-direction. This introduces the **axial frequency** [2],

$$\omega_z^2 = \frac{2qV_0}{md^2}. \tag{5}$$

We have argued that without the electric field, the particles would escape in the z-direction. However, if we did not have the magnetic field, the particles would escape in the xy-plane. This is a consequence of Gauss's law, which states that the field lines from the end caps above and below need to escape somehow.
This combination of $\mathbf{E}$ and $\mathbf{B}$ give rise to the effect of a **magnetron frequency** w_- and a **modified cyclotron frequency** w_+, as illustrated together with the the axial frequency w_z in FIG. 2. The expressions for $w_\pm$ are derived from solving the radial equations of motion [2], and as such they can be found as

$$\omega_\pm = \frac{\omega \pm \sqrt{\omega_0^2 - 2\omega_z^2}}{2}. \tag{6}$$

With the axial and cyclotron frequency well defined,

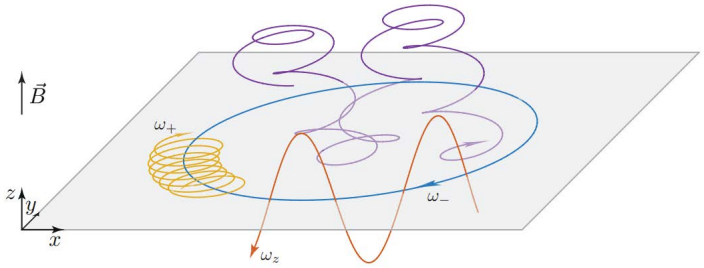

FIG. 2. The motion of a charged particle in a Penning trap, with the axial frequency ω_z (orange), magnetron frequency ω_- (blue), modified cyclotron frequency ω_+ (yellow) and the resulting combined motion (purple). The illustration is made by Klaus Baum [2].

we can now show how these quantities are related to the equations of motion for a charged particle in our Penning trap, from which we can calculate an explicit analytical solution for the particle trajectories.
Starting from Newton's second law

$$m\ddot{\mathbf{r}} = \sum_i F_i, \tag{7}$$

and the Lorentz force from equation 1, we have the relation

$$m\ddot{\mathbf{r}} = q\mathbf{E} + q\mathbf{v} \times \mathbf{B}, \tag{8}$$

where $\ddot{\mathbf{r}}$ denotes the second derivative of position, i.e. the acceleration, of the particle in three dimensions.
By using the expression for the electric field (4) and writing out the cross product, we can write out the expression explicitly in the x-, y- and z-direction as

$$m\ddot{x} = -\frac{qV_0}{d^2}x + q\dot{x} \times B_0\hat{e}_z \tag{9}$$

$$m\ddot{y} = -\frac{qV_0}{d^2}y + q\dot{y} \times B_0\hat{e}_z \tag{10}$$

$$m\ddot{z} = -\frac{2qV_0}{d^2}z + q\dot{z} \times B_0\hat{e}_z. \tag{11}$$

When we now divide both sides by m we recognize the expressions for ω_0 (2) and ω_z (5). By moving all the terms to the left hand side, we then get a familiar set of equations - namely, the equations of motion:

$$\ddot{x} - w_0\dot{y} - \frac{1}{2}\omega_z^2 x = 0 \tag{12}$$

$$\ddot{y} + w_0\dot{x} - \frac{1}{2}\omega_z^2 y = 0 \tag{13}$$

$$\ddot{z} + \omega_z^2 z = 0. \tag{14}$$

While the solution of the motion in the z-direction is easy to derive, equation (12) and (13) are coupled. To solve these, we must therefore introduce a complex function $f(t) = x(t) + iy(t)$ which has the following properties:

$$\dot{f} = \dot{x} + i\dot{y} \tag{15}$$

$$i\dot{f} = i\dot{x} - \dot{y} \tag{16}$$

$$\ddot{f} = \ddot{x} - \ddot{y}. \tag{17}$$

By subtracting equation (12), by i multiplied with equation (13), sorting the terms yield the following expression:

$$\ddot{x} - i\ddot{y} + \omega_0(i\dot{x} - \dot{y}) - \frac{1}{2}\omega_z^2(x + iy) = 0. \tag{18}$$

We can now recognize the terms from equation (15), (16) and (17). From here, we rewrite the equations of motion (12) and (13) as

$$\ddot{f} + i\omega_0\dot{f} - \frac{1}{2}\omega_z^2 f = 0. \tag{19}$$

This equation has a general solution

$$f(t) = A_+ e^{-i(\omega_+ t + \phi_+)} + A_- e^{-i(\omega_- t + \phi_-)}, \tag{20}$$

where $A_\pm$ are positive amplitudes, and $\phi_\pm$ are constant phases.
For the case

$$\omega_0^2 > 2\omega_z^2 \tag{21}$$

we have from equation (6) that $\omega_\pm$ are real. Using this logic, we know that $x(t)$ and $y(t)$ can therefore be rewritten from (20) using Euler's formula, $e^{-it} = \cos(t) - i\sin(t)$, as

$$x(t) = A_+ \cos(\omega_+ t + \phi_+) + A_- \cos(\omega_- t + \phi_-) \tag{22}$$

$$y(t) = -A_+ \sin(\omega_+ t + \phi_+) - A_- \sin(\omega_- t + \phi_-). \tag{23}$$

These equations are shown in FIG. 3 where we see that the movement in the xy-plane is bound to a circle with a constant radius R. In the first part of our simulation

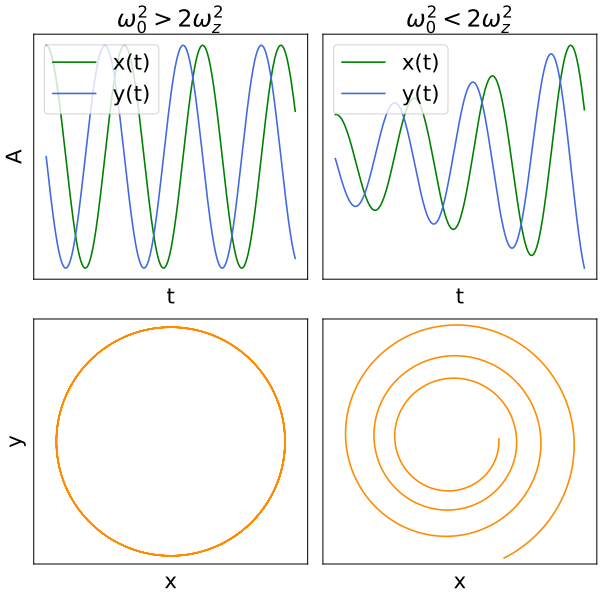

FIG. 3. First row: equation (22) and (23) visualized for the two cases when ω_0^2 is greater or less than $2\omega_z^2$. From the left plot we see that $x(t)$ and $y(t)$ are oscillating with stable amplitudes, while the amplitudes are increasing in the right plot. Second row: The resulting movement in the xy-plane. The trajectory is bound for the case $\omega_0^2 > 2\omega_z^2$, while the trajectory is increasingly moving outwards when $\omega_0^2 > 2\omega_z^2$.

of the Penning trap, we will consider a singly charged particle, a Ca^+-ion with the initial conditions

$$x(0) = x_0, \qquad \dot{x}(0) = 0,$$
$$y(0) = 0, \qquad \dot{y}(0) = v_0,$$
$$z(0) = z_0 \qquad \dot{z}(0) = 0,$$

which gives the specific solution in the x- and y-direction as equation (22) and (23) with

$$A_+ = \frac{v_0 + \omega_- x_0}{\omega_- - \omega_+}, A_- = -\frac{v_0 + \omega_+ x_0}{\omega_- - \omega_+},$$
$$\phi_+ = 0, \phi_- = 0,$$

while the solution for $z(t)$ becomes

$$z(t) = z_0 \cos(\omega_z t). \tag{24}$$

By looking at equation (23) at the time when $y(t)$ is zero, i.e. when the sine-terms are 0 and the cosine-terms are ± 1, we see that the maximum radius is found when

$$\omega_+ t + \phi_+ = \omega_- t + \phi_-,$$

or in other words, when the radius is $R_{max} = A_+ + A_-$. Similarly we find the minimum radius when

$$\omega_+ t + \phi_+ = -(\omega_- t + \phi_-),$$

as $R_{min} = |A_+ - A_-|$.

For the case $\omega_0^2 < 2\omega_z^2$ we have from equation (6) that $\omega_\pm$ are imaginary numbers, and the expression $f(t)$, when neglecting constant phases and amplitudes, will then be in the form

$$e^{-i\omega_\pm} = e^{-i[\mathrm{Re}(\omega_\pm)+i\mathrm{Im}(\omega_\pm)]t} = e^{-i\mathrm{Re}(\omega_\pm)t} \cdot e^{\mathrm{Im}(\omega_\pm)t}, \tag{25}$$

where the last expression in the multiplication will grow to ∞ as $t \to \infty$, causing $x(t)$ and $y(t)$ to oscillate between $\pm\infty$. This results in an unbounded movement for the charged particle in the xy-plane, as shown in Fig. 3.
To get a stable, bounded movement we therefore need the constraint $\omega_0^2 \geq 2\omega_z^2$, which expressed using the Penning trap parameters and particle properties becomes

$$\frac{q}{m} \geq \frac{4V_0}{d^2 B_0^2}. \tag{26}$$

We will use singly charged Ca^+ ions with mass and charge listed together with the Penning trap parameters in table I.

TABLE I. The values we will be using for the Penning trap parameters (B_0, V_0, d) and the Ca^+ particle properties (q, m) using the units micrometer, microseconds, atomic mass and elementary charge.

Quantity	Value	unit
q	1	e
m	40.078	u
B_0	9.65×10^1	$\frac{\mathrm{u}}{(\mu\mathrm{s})\,\mathrm{e}}$
V_0	2.41×10^6	$\frac{\mathrm{u}\,(\mu\mathrm{m})^2}{(\mu\mathrm{s})^2\,\mathrm{e}}$
d	500	μm

When using multiple particles in our Penning trap, we also need to consider the **Coulomb forces** acting between the particles. For two particles with charge q separated by a vector $\mathbf{r}$ we find the Coulomb force as

$$F_C = k_e \frac{q \cdot q}{|\mathbf{r}|^3}\mathbf{r}, \tag{27}$$

where $k_e = 1.38935333\ \frac{\mathrm{u}(\mu\mathrm{m})^3}{(\mu\mathrm{s})^2\mathrm{e}^2}$ is the Coulomb constant. The equations of motion for particle i then needs to include the forces from all the other particles as

$$\ddot{x}_i - \omega_{0,i}\dot{y}_i - \frac{1}{2}\omega_{z,i}^2 x_i - k_e \frac{q_i}{m_i}\sum_{j\neq i} q_j \frac{x_i - x_j}{|\mathbf{r}_i - \mathbf{r}_j|^3} = 0, \tag{28}$$

$$\ddot{y}_i + \omega_{0,i}\dot{x}_i - \frac{1}{2}\omega_{z,i}^2 y_i - k_e \frac{q_i}{m_i}\sum_{j\neq i} q_j \frac{y_i - y_j}{|\mathbf{r}_i - \mathbf{r}_j|^3} = 0, \tag{29}$$

$$\ddot{z}_i + \omega_{z,i}^2 z_i - k_e \frac{q_i}{m_i}\sum_{j\neq i} q_j \frac{z_i - z_j}{|\mathbf{r}_i - \mathbf{r}_j|^3} = 0. \tag{30}$$

As these equations are quite complicated, we will not attempt an analytical solution, but instead use numerical algorithms to determine the particle trajectories.

B. Algorithms

We will use two different numerical integration methods to determine the trajectories in the Penning trap system; the Forward Euler method and the Runge Kutta method.

1. *Forward Euler*

The Forward Euler method (FE) is a simple first-order, single-step method where we take use of the known gradient $\frac{dy}{dt} = f(t, y)$ at a single point

$$\frac{y(t+h) - y(t)}{h} + \mathcal{O}(h) = f(t, y), \tag{31}$$

where h is the step size and $\mathcal{O}(h)$ denotes the local error of order h.
Rearranging for $y(t+h)$ we get

$$y(t+h) = y(t) + hf(t, y) + \mathcal{O}\left(h^2\right). \tag{32}$$

When we now use discrete points, $y(t) \to y_i$ and $f(t, y) \to f_i$, and leave out the $\mathcal{O}\left(h^2\right)$ term, we get the approximation

$$y_{i+1} = y_i + hf_i. \tag{33}$$

As the local error of this approximation is $\mathcal{O}\left(h^2\right)$ the global error is $\mathcal{O}\left(h\right)$.
For the particles, the known function f is the acceleration which we can calculate from the position- and velocity-dependent force acting on them. To derive the position, we first need to calculate the velocity with FE, before using this to find the position.
The FE algorithm we will be using is shown in algorithm 1, where we have used n steps of step size h, and the notation F_i as the force at time step i. We say that the algorithm is single-step as the position is calculated using only one step.

Algorithm 1 Forward Euler integration

procedure FORWARD EULER(n, h, F_i, m, v_0, r_0)
  for $i = 0, 1, \ldots, n$ **do**
    $a_i \leftarrow F_i/m$ ▷ Assign a_i from Newtons second law
    $v_{i+1} \leftarrow v_i + ha_i$ ▷ Evolve v_i one time step
    $r_{i+1} \leftarrow r_i + hv_i$ ▷ Evolve r_i one time step

2. Runge-Kutta

The 4th order Runge-Kutta method (RK4) is a more accurate method compared to the FE method, as the number 4 indicate the $\mathcal{O}(h^4)$ global error. However, the computational cost is substantially greater.
In this method, we evaluate the gradient at four different times, assigned to four k_i with $i \in 1, 2, 3, 4$ values, and use a weighted sum of these to evaluate the evolution for one step in time.
The first k-value is calculated at the beginning of the time step, as we do in the FE method. The second and third k-values are calculated at the middle of the time step, while the fourth is calculated at the end. From this we get a more detailed measurement of the gradient along the step size, compared to just having one estimate as in the FE method.
In the three last k's, we also take use of the previous k-value to evaluate the known function f. This can be seen as a predictor-corrector method, were we use the already calculated quantities to determine the next.
To illustrate, k_2 at iteration number i is calculated using an f at the y-value $y_i + \frac{1}{2}k_1$.
As the acceleration calculated from the force, i.e. the known function f, is both velocity and position dependent, we need to calculate the acceleration at position i for k_2 from $a(v_i + \frac{1}{2}k_1, r_i + \frac{1}{2}k_1)$.
The final position and velocity is calculated from a weighted sum of the four k's, where the weights can be derived [3] using the Fundamental Theorem of Calculus and Simpsons's rule.
The explicit Runge-Kutta algorithm is shown in algorithm 2.

Algorithm 2 4th order Runge-Kutta integration

procedure RUNGE-KUTTA(n, h, F_i, m, v_0, r_0)
  for $i = 0, 1, \ldots, n$ **do**
    $k_{v,1} \leftarrow ha(r_i, v_i)$ ▷ Calculate k_1
    $k_{r,1} \leftarrow hv_i$
    $k_{v,2} \leftarrow ha(r_i + \frac{1}{2}k_{r,1}, v_i + \frac{1}{2}k_{v,1})$ ▷ Calculate k_2
    $k_{r,2} \leftarrow h(v_i + \frac{1}{2}k_{v,1})$
    $k_{v,3} \leftarrow ha(r_i + \frac{1}{2}k_{r,2}, v_i + \frac{1}{2}k_{v,2})$ ▷ Calculate k_3
    $k_{r,3} \leftarrow h(v_i + \frac{1}{2}k_{v,2})$
    $k_{v,4} \leftarrow ha(r_i + k_{r,3}, v_i + k_{v,3})$ ▷ Calculate k_4
    $k_{r,4} \leftarrow h(v_i + k_{v,3})$
    $v_{i+1} \leftarrow v_i + \frac{1}{6}(k_{v,1} + 2k_{v,2} + 2k_{v,3} + k_{v,4})$ ▷ Evolve
    $r_{i+1} \leftarrow r_i + \frac{1}{6}(k_{r,1} + 2k_{r,2} + 2k_{r,3} + k_{r,4})$

C. Simulation

The primary focus of our simplified model is to simulate the motion of singly-charged calcium-ions in different conditions, and then extrapolate the importance of various attributes of the Penning trap.
Using the derived equations above, coupled with the aforementioned numerical methods, we can then apply them to find the motion of the confined particles. Since two numerical methods are implemented into our model, we find it salient to choose the method that corresponds the most to the analytical solutions - this is decided by running both numerical methods for **one** particle, without any Coulomb interactions or time-dependency for our electric potential V.

Upon finding the superior numerical method, we can then attempt to simulate more particles, with or without any additional conditions - such as the Coulomb interaction, or time-dependent electric potential. Implementing a method to include the additional conditions when calculating the total force on the particles, meaning from both the surrounding fields and particles, can be done in a variety of different ways.
In our model, we choose to implement these conditions into existing methods made for calculating the total force on our particles - the caveat being that they are only included if their booleans allow them.
Having included the additional conditions into our model, we then turn our sights towards simulating more aspects of our simplified model; such as the trajectories in the phase space, and in three-dimensional Euclidean space.
Further, we also want to consider the impact our choice of time-steps has on our simulation. We do this for both numerical methods. By simulating one particle for different time-steps, we can then weigh whether increasing the time-steps affects our model negatively or positively, and whether the inferior method is still applicable in certain ranges of time-steps. Comparing the impacts on both methods is done by plotting the relative error, after which we for each numerical method calculate the error convergence rate, given by

$$r_{err} = \frac{1}{3}\sum_{k=2}^{4} \frac{\log(\Delta_{max,k}/\Delta_{max,k-1})}{\log(h_k/h_{k-1})}, \tag{34}$$

where

$$\Delta_{\max,k} = \max_i |\mathbf{r}_{i,\text{exact}} - \mathbf{r}_i| \tag{35}$$

is the absolute error for a choice of simulation step k, and h_k is the corresponding step-size for a choice of simulation step k; found by dividing the total simulation time of $50\mu\,s$ by the choice of simulation steps, n_k.

Lastly, another aspect of the Penning trap we will attempt to study with our model, is how the particle orbits can change when introducing a time dependent electric potential with a given frequency ω_V.
When the electric potential varies with time, i.e. when the electric field strength varies with time, it can constructively or destructively change the kinetic energy of the particles, depending on how well ω_V matches the frequencies ω_z, ω_+ and ω_- which describes the particle motion, as seen in FIG. 2.
This is because the magnetic field causes a coupled motion, mentioned in equation (12) and (13), which give rise to the possibility of energy transfer between the modes. This energy-transfer will be negligible for most choices of ω_V, but when it matches the frequency of the particle motion, it will cause the particles to quickly gain kinetic energy. When reaching this **resonance frequency**, the particles will be forced in to greater orbits, and eventually be sent out of the Penning trap.
By introducing the time dependent potential

$$V_0 \to V_0(1 + f\cos(\omega_V t), \tag{36}$$

where f is the amplitude, we run tests using frequencies in the range $\omega_V \in (0.2, 2.5)$ MHz for three different amplitudes $f = 0.1, 0.4, 0.7$, and see how well the particles escape the trap.
We run the tests over 500 μs using 25 particles with and without Coulomb interactions. Since this already takes around 5 minutes total, we limit ourselves to this number of particles, as we it seems that this gives decent results. After finding the resonance frequency, we attempt to perform a fine-grained frequency-scan around this frequency, both including Coulomb interactions and not.

III. RESULTS AND DISCUSSION

Our first objective is to compare the accuracy of our different numerical methods, i.e. the aforementioned Forward-Euler (FE) and RungeKutta4 (RK4). As such, we then run our simulation for one particle using both methods, without any Coulomb interaction, and compare it to the analytical solution. Running our simulation with these conditions, yielded the plots of z and x over time shown in FIG.4 and FIG.5.
From these we see that the RK4 method aligns well with the analytical solution, and the motion of $z(t)$ seems reasonable for the value of $\omega_z = 0.69$. In comparison we see that the FE method deviates somewhat from the analytical solution for $z(t)$, and is noticeably different for $x(t)$. With this in mind, we can then move on and attempt to model the position-velocity phase space of the x and z components using only the RK4 method, as shown in

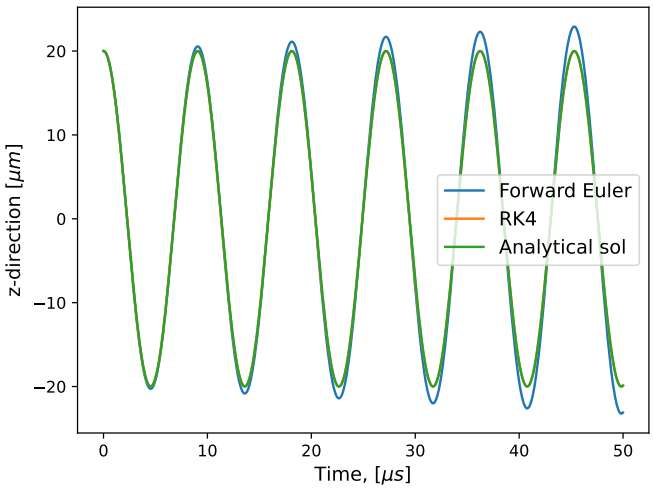

FIG. 4. Comparison of results from numerical methods against the analytical solution for the motion of the particle along z-axis over time. The blue line shows our results from the FE-method, the orange line our results from the RK4-method, and the green line is the analytical baseline (24) for comparison. The RK4 method is overlapping with the analytical solution.

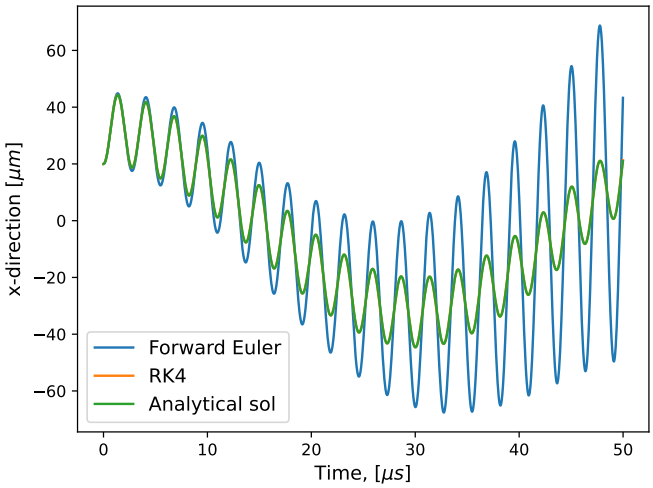

FIG. 5. Comparison of results from numerical methods against the analytical solution for the motion of the particle along x-axis over time. Similarly, the blue line shows our results from the FE-method, the orange line our results from the RK4-method, and the green line is our analytical baseline (22) for comparison. The RK4 method is overlapping with the analytical solution.

FIG.6. and FIG.7.
From the phase space of the z-component, we see that the trajectory forms a closed loop for both particles. This is expected as the movement in the z-direction only con-

sists of one continually oscillation component, the axial movement with frequency ω_z, as shown in FIG. 2.
From the same figure, we see that the movement in the x-direction consists of two components, the magnetron motion with frequency ω_- and the cyclotron motion with frequency ω_+. The more complicated phase space for the x-component is therefore expected.

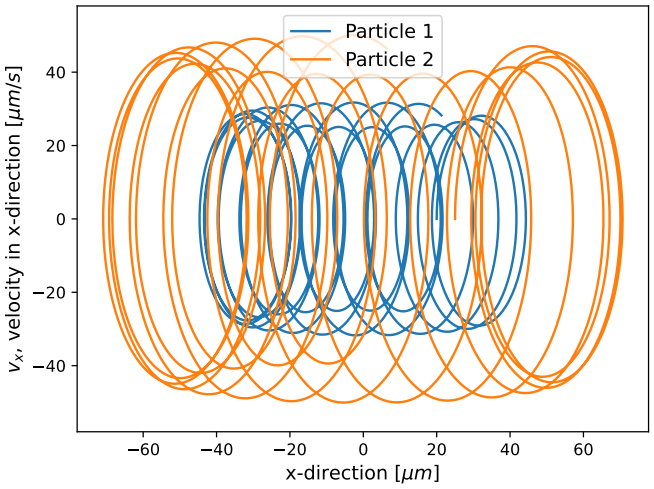

FIG. 6. Plot of the position-velocity phase-space in the x-direction. The blue line represents the motion of the first particle, the orange the motion of the second particle.

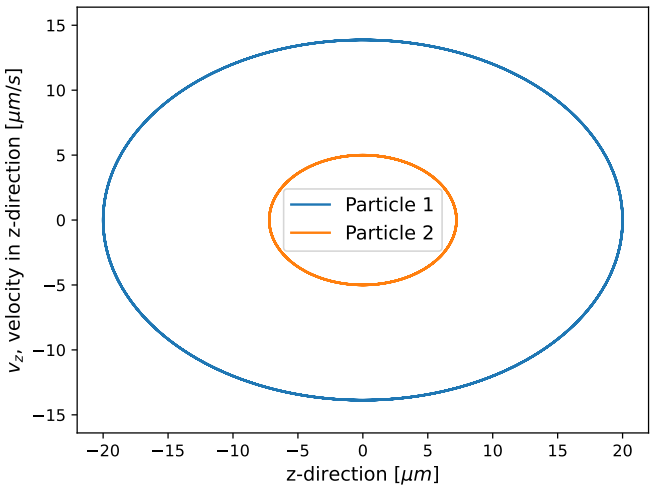

FIG. 7. Plot of the position-velocity phase-space in the z-direction. The blue line represents the motion of the first particle, the orange the motion of the second particle.

Having stated that the RK4 method seems more accurate than the FE method, we now perform an error-analysis of the two and compare how the choice of time steps affect the relative error, $\mathbf{r_i}$, and error convergence rate, $\mathbf{r_{err}}$ (34).
By plotting the relative error over time, we can see how it behaves for each numerical method, and more clearly see the accumulation of the errors in the FE-method. The results can be found in the plots given by FIG.8. and FIG.9.
From the plots, we see that the FE method quickly reaches a relative error of 10^{-2} and continues to grow throughout the simulation, while the RK4 method stays between 10^{-2} and 10^{-3}. This proves RK4 to be the superior numerical method in terms of accuracy.

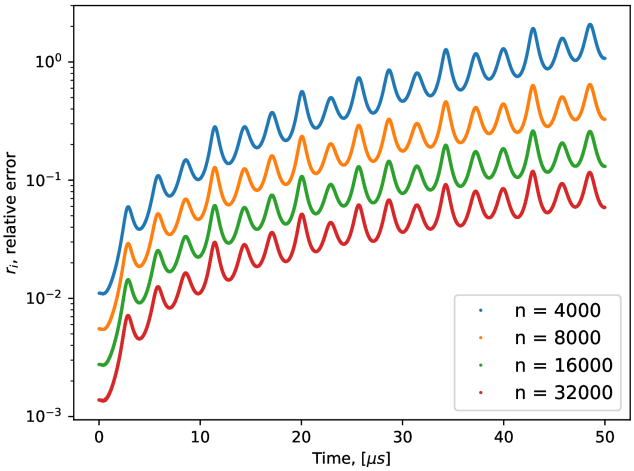

FIG. 8. Comparison of results from the FE-method for each choice of simulation steps for our model. The blue line represents $n_1 = 4000$, the orange line $n_2 = 8000$, the green line $n_3 = 16000$, and the red line $n_4 = 32000$. Here the y-axis was set to a logarithmic scale, such that any increase or decrease in the relative error can more easily be seen.

Using the data from these plots yielded the error convergence rates presented in TABLE III. The results presented in this table, make it apparent that the FE-method accumulates errors in a way that makes it substantially inferior to the RK4-method at higher choices of simulation steps. As such, we only make use of the RK4-method for any further simulations of our simplified model.

Method	$\mathbf{r_{err}}$
Forward-Euler	$1.39656 \approx 1.4$
RungeKutta4	$0.99505 \approx 1.0$

TABLE II. Table containing the error convergence rates, $\mathbf{r_{err}}$, for each method used to numerically derive the particles motion.

Repeating the previous simulations for the ion's motion with two charged particles, while varying the condi-

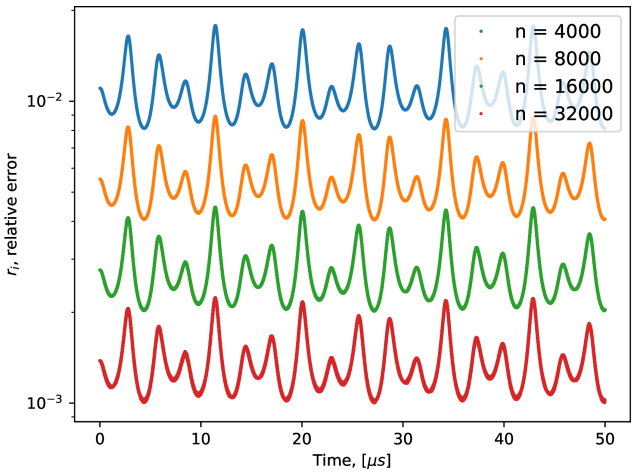

FIG. 9. Comparison of results from the RK4-method for each choice of simulation steps for our model. Similarly, the blue line represents $n_1 = 4000$, the orange line $n_2 = 8000$, the green line $n_3 = 16000$, and the red line $n_4 = 32000$. Here the y-axis was set to a logarithmic scale, such that any increase or decrease in the relative error can more easily be seen.

tion of there being any Coulomb interaction between the charged particles, yields the plots of the movement in the xy-plane presented in FIG.10., and FIG.11.

Looking over these plots reveals that something is not quite right with the model; most notably, the fact that none of the simulations where the Coulomb interactions are included, properly simulate the motion of the charged particles.

There are a few aspects of the simplified model where we suspect this fault lies, however all of them stem from the assumption that our implementation of the Coulomb interaction is not updating correctly in our applied numerical methods.

After assessing our code, we posit two possible solutions to this fault: to rewrite the implementation of the total forces acting on the particle and to store the force as a temporary variable for each simulation-step in our numerical methods. Several attempts have been made to locate and rectify this fault, but to no avail.

By explicitly writing out the forces calculated at each position and velocity, the methods for calculating the forces seems to give correct results. However, the way that the Coulomb interactions effects the particles position and velocity seems to be faulty.

Since we know that the force calculation and the RK4 method gives accurate results without Coulomb interactions, a possible fault could be in how the methods for calculating the particle-interaction forces, explicitly the methods `force_particle` and `total_force_external` found in the GitHub repository, interacts with the other methods.

Upon checking each term in the expressions for the force in our model, we suspect that the way we have implemented our numerical method causes the velocity in equation (1) to approach very small values for some velocity-components, and very large for others - causing the values for the magnetic field to being faulty as well, and there by causing an unbounded movement in the xy-plane.

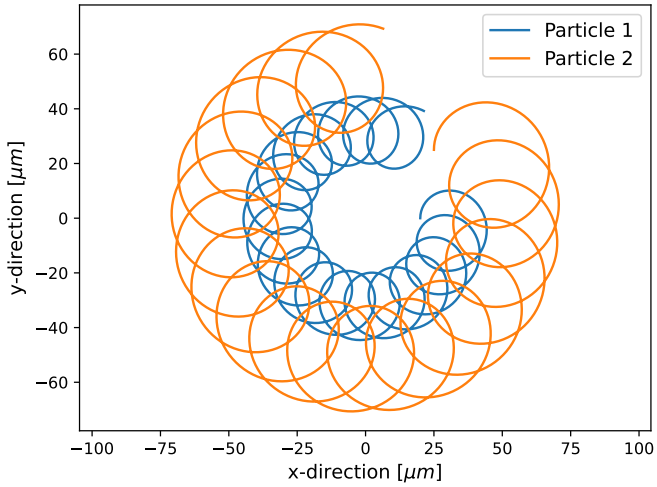

FIG. 10. Plot of the two charged particles' motion in the xy-plane made by our simulated model of the Penning trap. This simulation has no Coulomb interaction.

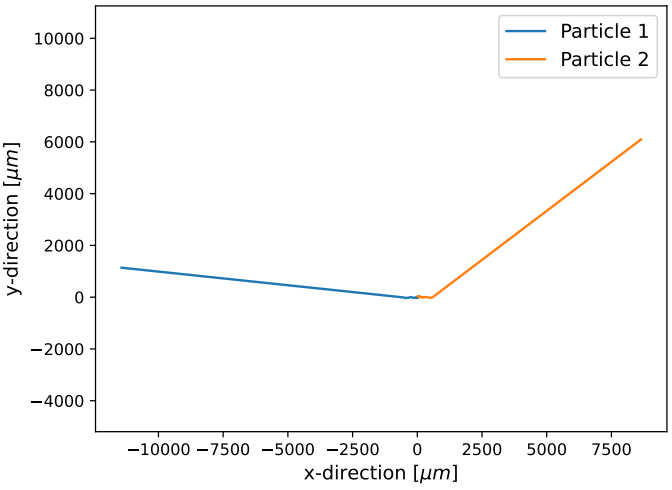

FIG. 11. Plot of the two charged particles' motion in the xy-plane made by our simulated model of the Penning trap. This simulation has Coulomb interaction included, and is clearly different from the case where no such forces are included.

By zooming in at the origin, yields the plot shown in FIG.12. A somewhat familiar pattern appears at the center, but something is obviously wrong as the trajectory

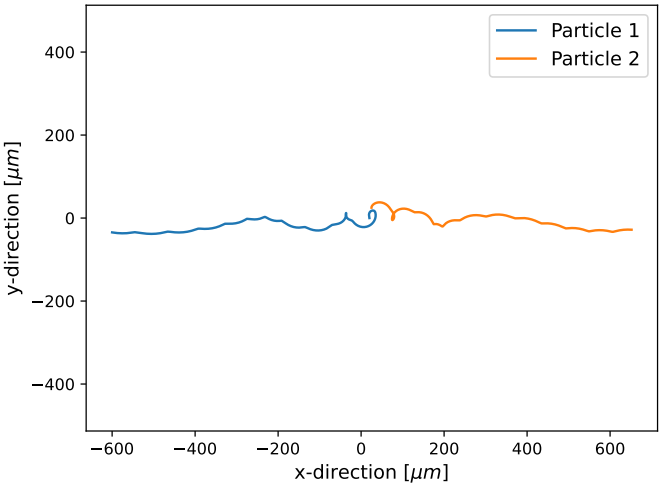

FIG. 12. Plot of the charged particles' motion in the xy-plane of our simulated model of the Penning trap. The only additional condition being enforced here is the Coulomb interaction. Here we zoom in on the initial "knot" of the particles motion, and we see a rather different trajectory compared to when no Coulomb forces are included.

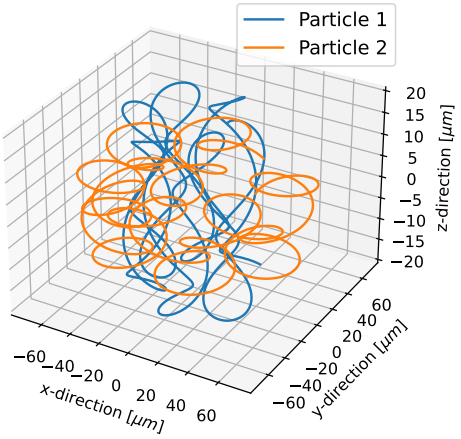

FIG. 13. 3D-plot of the motion of the two charged particles, using the RK4-method and no additional enforced conditions. We recognize these trajectories from the combined motion presented in FIG. 2.

seems to only be affected by the Coulomb interactions as it is no longer rotating around the center of the trap.
Seeing as we are unable to rectify this fault at the time of this report, the remaining plots of the particles' motion, are the results of simulations done without considering the effects of the Coulomb interactions.
Plotting the motion of the charged particles in three-dimensions, yields the plot shown in FIG. 13. These motions are similar to the expected combined motion from FIG. 2.

From the study of how the time dependent electric potential (36) effects the particle orbits, we get the plots in FIG. 14 showing the fraction of particles still inside the Penning trap after the simulations, as a function of the applied frequency ω_V.
From this we see that the fraction of particles trapped is clearly affected for certain frequencies, while for others all the particles remain inside.
Explicitly, we see that the particles are being excited out of the Penning Trap around the frequencies 0.7 MHz, 1.4 MHz and 2.2 MHz, in addition to 0.4 MHz for the frequency $f = 0.7$.
By comparing these to the frequencies ω_z (5) and $\omega_\pm$ (6) related to the particle motion

$$\omega_z = 0.694 \text{ MHz}, \tag{37}$$
$$\omega_+ = 2.303 \text{ MHz} \tag{38}$$
$$\omega_- = 0.104 \text{ MHz} \tag{39}$$

where we have used the values from table I, we see that the resonance frequencies appear around one, two, and three times ω_z for all the three amplitudes, and about

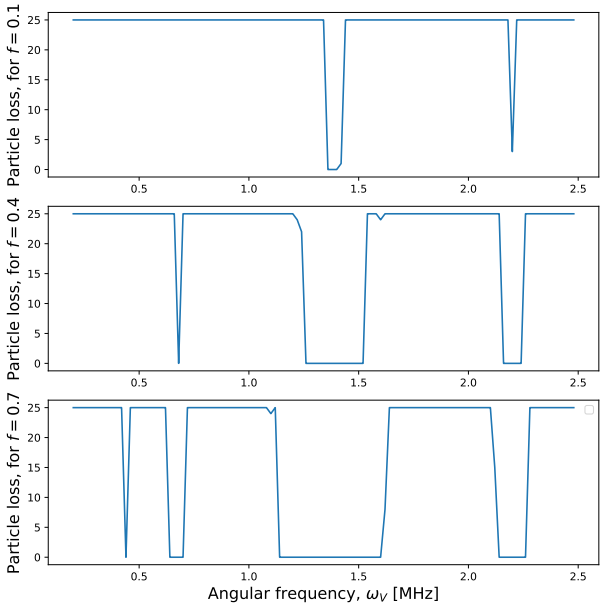

FIG. 14. Plot showing the fraction of trapped particles as a function of the applied potential-frequencies in the range $\omega_V \in (0.2, 2.5)$ MHz in steps of 0.02 MHz for three different amplitudes $f = 0.1, 0.4, 0.7$, after a simulation lasting 500 μs. The particles trapped reduces rapidly around the frequencies $\omega = 0.7, 1.4, 2.2$ MHz for all amplitudes, and $\omega = 0.4$ for the $f = 0.7$.

four times ω_- for the biggest amplitude.
This implies that the applied electric field particularly affects the axial motion with frequency ω_z, and to some extent the magnetron motion with frequency ω_-.
This effect is increased around the resonance frequencies

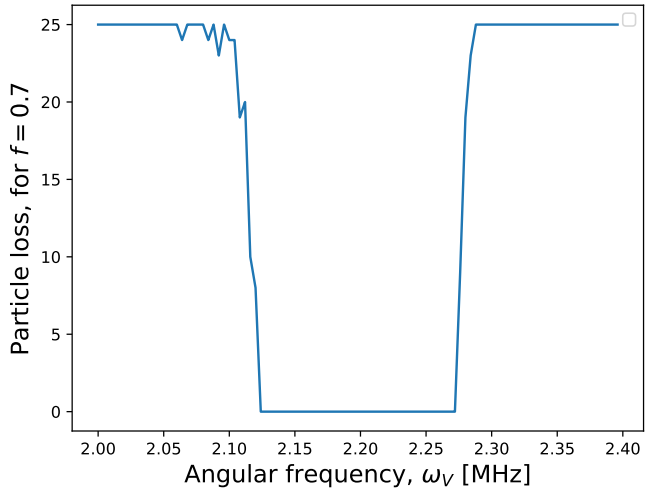

FIG. 15. A fine grained scan of the applied frequencies in the range $\omega_V \in (2.0, 2.4)$ MHz in steps of 0.04 MHz using an amplitude of $f = 0.7$, after a simulation lasting 500 μs. It is clear that the frequencies around the resonance frequency make the particles leave the trap within the duration of the simulation.

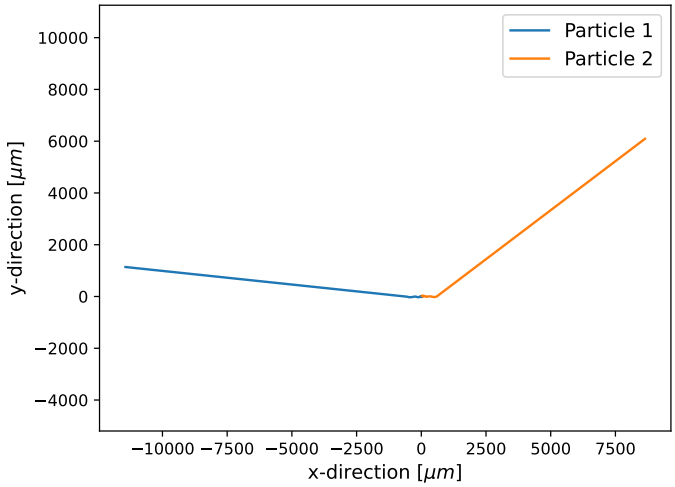

FIG. 16. Plot of the charged particles' motion in the xy-plane of our simulated model of the Penning trap when including a time-dependent electric potential and Coulomb interactions. The result is not noticeably different for the case of a constant electric potential.

when the amplitude of the applied potential is increased, as the energy transfer between the different modes of motion now will be greater. This means that a frequency further away from the resonance frequency will increase the energy of the particles more, given a higher potential-amplitude than a lower potential-amplitude.

As the measured resonance frequencies seems to be multiples of the particle-frequencies, we could argue that we have got reasonable results.

By performing a frequency scan with a more fine-grained interval of ω_V around the resonance frequency 2.2 MHz, we get the plot in FIG. 15 which underlines how the applied electric potential can be used to excite particles from the trap.

By applying the time dependent varying potential for only two particles when also including the Coulomb interactions, we do not really see a difference compared to when the presence of electric potential is not enforced. This is shown in FIG. 16. As discussed, there seems to be an error in the implementation of the Coulomb forces between the particles, and the results found where the condition of the Coulomb interaction is applied, therefore seems unreasonable.

IV. CONCLUSION

Our study of the motion of singly-charged calcium ions in a Penning trap yielded valuable insights into the complex behavior of these particles under various conditions. By employing two numerical methods, the Forward-Euler and RungeKutta4, we have through a meticulous examination of the particles' trajectories expanded our understanding of the fundamental principles that govern the motion of particles confined by electromagnetic fields.

Although we were not able to correctly implement a method to enforce a Coulomb interaction between the charged particles, and ended up producing an array of faulty plots, we managed to implement a method for the time-dependent electric potential. Further, the introduction of this method, brought about an understanding how an oscillating electric can be applied to determine the resonance frequencies of the Penning trap-particle system, which can be used to among other things determine the mass of unknown particles, i.e. the aforementioned mass spectrometry. For future work, to ensure more accurate results and a more realistic model of the Penning trap, a correct implementation of the Coulomb interaction should be added.

An essential part of our investigation was the comparison of error convergence rates between our choices of numerical methods, namely the FE and RK4-methods. We found that the RK4 consistently outperformed FE in terms of accuracy, particularly when dealing with larger choices of simulation steps. This emphasizes the importance of selecting an appropriately sturdy numerical method when simulating the motion of charged particles in complex environments - such as the Penning trap.

In summary, having studied the behavior of charged particles in a Penning trap has contributed to a deeper understanding of the behavior of charged particles in particle traps. We have shed light on the intricate play of forces acting among the particles, and between the particles and the surrounding fields. Having delved into the

realm of particle traps, has given us valuable insights into the dynamics of such a system, and the importance of numerical methods when it comes to simulating one.

---

[1] E.K. Anderson. Observation of the effect of gravity on the motion of antimatter. *Nature*, 621:716–722, 2023.
[2] K. Baum. Cyclotron frequency in a Penning trap. https://www.physi.uni-heidelberg.de/Einrichtungen/FP/anleitungen/F47.pdf, 2022. Accessed on October 24, 2023.
[3] M.H Jensen. *Computational Physics*, chapter 8, pages 250–252. Department of Physics, University of Oslo, 2015.